

## Chapter

# SiO<sub>2</sub>-Based Materials for Immobilization of Enzymes

*Crina Anastasescu, Mihai Anastasescu, Ioan Balint  
and Maria Zaharescu*

## Abstract

It is well known that SiO<sub>2</sub>-based nanomaterials were widely used as support material for many chemically active species but also for compounds with biological activity such as antibodies and enzymes, due to their lack of toxicity and high surface area. The hybrid materials resulted from associating enzymes with various morphologies of SiO<sub>2</sub> inorganic matrix, especially obtained by sol-gel method, are meant to develop a higher enzymatic activity and increased lifetime but also the recovery and reutilization advantage. The present contribution emphasized the synthesis of SiO<sub>2</sub> nanomaterials with different morphologies and their physicochemical characteristics including biocatalytic activity of immobilized enzymes on simple SiO<sub>2</sub>. The morphology-dependent behavior of SiO<sub>2</sub> inorganic carriers obtained by sol-gel method was also emphasized. Accordingly, SEM investigations, nitrogen sorption, electrokinetic potential, and spectroscopic measurements are presented. p-Nitrophenyl acetate (p-NPA) was used for testing the enzymatic activity of as-prepared lipase-SiO<sub>2</sub> hybrid materials.

**Keywords:** SiO<sub>2</sub>, sol-gel, enzymes, immobilization

## 1. Introduction

New multifunctional materials are required as practical solutions for competitive, affordable, and environmentally friendly technologies from industrial and health-care areas. These should be also able to sustain and preserve various ecosystems and an appropriate quality of human life, gathering resources from border scientific fields: materials science, bioremediation, biocatalysis, and biomedicine [1].

Silica is largely studied material with high chemical and thermal stability, nontoxic and non-expensive, which can display a huge variety of morphologies, not only in natural state but also obtained by various synthetic routes. For these reasons, silica with high surface area (MCM 41, SBA 15) is intensively used as support for chemical active species [2] but also as inorganic host in hybrid complex for biological active compounds (enzymes) [3], especially those obtained in mild conditions, by sol-gel method [4]. These materials are recognized as appropriate carriers for biological compounds, preserving or increasing their intrinsic features [5]. In addition, tubular morphology of silica allows custom modification/functionalization of internal/external surfaces with chemical (metals, oxides) and biological (enzymes, antibodies) active compounds [6].

In this work we review various SiO<sub>2</sub> morphologies obtained during our material development researches, pointing out their peculiar properties and advantages related to the immobilization of enzymes for potential practical applications.

## 2. Sol-gel synthesis of different SiO<sub>2</sub> structures obtained by sol-gel method: sphere-, tube-, and veil-type morphologies

Our previous works reported sol-gel synthesis and characterization of SiO<sub>2</sub> matrices with different morphologies (nanotubes, spheres, and veils) but also emphasized the multifunctional behavior of the as-obtained SiO<sub>2</sub> materials, from the perspective of their chemical and biological activity. Firstly, spherical particles and hollow nanotubes with open ends, square shape, and high surface area (300 m<sup>2</sup>/g), [7, 8] were obtained at room temperature and atmospheric pressure, using DL tartaric acid as in situ generated template. The catalytic [9] and photocatalytic [10] activities of platinum-modified SiO<sub>2</sub> nanotubes and spheres were further investigated and proven to be dependent on morphology of SiO<sub>2</sub> matrix which bears (supports) the metallic active phase. SiO<sub>2</sub> veils have been also obtained, and their composites have been used as support for platinum electrocatalyst [11].

Improvement of in situ generated template-assisted SiO<sub>2</sub> synthesis and appropriate post-synthesis treatments allowed us to obtain nanotubes with intrinsic photo- and electrochemical activity due to high density of oxygen-related lattice defects [12, 13] but also to reveal the distinctive capacity of highly defected SiO<sub>2</sub> and its composite SiO<sub>2</sub>-TiO<sub>2</sub> to generate reactive oxygen species (ROS) with potential applications in biology and medicine [14].

SiO<sub>2</sub> materials (nanotubes) have been proven to be biologically active for bioremediation processes, showing bactericidal and bacteriostatic effects on halotolerant microorganisms [15]. These type of materials have been successfully used as inorganic carriers in hybrid complex with enzymes [16], the enzymatic activity of the complex being dependent on morphological and textural properties of SiO<sub>2</sub> matrices [17].

Generally, sol-gel synthesis of tubular SiO<sub>2</sub> materials was conducted in line with Nakamura and Matsui's work [18], modifications of synthetic procedure being done in respect to particular applications.

Thin and larger SiO<sub>2</sub> nanotubes in addition to spherical SiO<sub>2</sub> are meant to function as inorganic host for immobilized enzymes, and, accordingly, their previously synthesis has been reported [7, 17]. Better control of synthesis conditions allowed an optimization of their morphology and structure, in order to be appropriate for an inorganic carrier. Generally, these materials are resulting from a template-assisted sol-gel process, consisting in hydrolysis and condensation reactions conducted in the presence of DL tartaric acid, in respect to well-defined and well-controlled synthetic parameters which will be exposed in what comes. By selecting proper temperature, concentration of started solution, and in situ organic template development, not only morphological changes (observed in SEM captured images) can be induced but also structural ones, resulting in highly defected surfaces with increased chemical reactivity [12].

In this sense, we used a mixture of tetraethyl orthosilicate (TEOS) (Alfa Aesar, 99%), absolute ethanol (Riedel-de Haen), ammonia (25% w/w aq. Alfa Aesar), and DL tartaric acid (TA) as internal templating agent. The involved molar ratio was 1 (TEOS):0.07 (tartaric acid):43 (ethanol):36 (H<sub>2</sub>O), at 20°C. A subsequent addition of ammonia (25%), drop by drop, triggers the formation of the final synthesis product, a white and dense suspension being observed. The whole synthetic procedure is performed in mild conditions, at room temperature (25°). One hour aging time is allowed followed by filtering, washing with ultrapure water (Milli-Q system, 18 MΩcm), and drying at 100°C for 3 hours. Typically, the post-synthesis thermal treatment involves calcination for 3 h at 500°C with a heating rate of 0.5°C/minute (**Figure 1**).

This synthesis route leads to hollow and large nanotubes, together with a minor percent of spherical particles. The sample will be denoted in what comes as SiO<sub>2</sub>TL sample (TL meaning large tubes) (**Figure 3**).

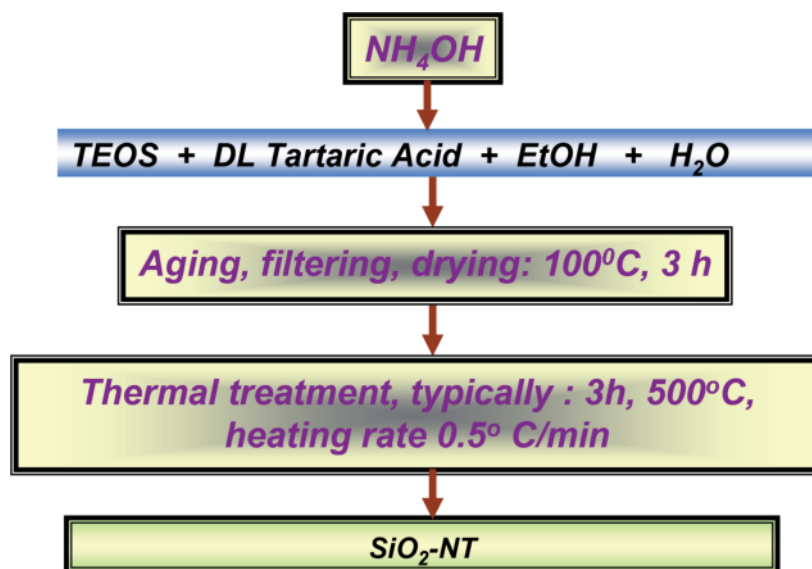


**Figure 1.** Schematic representation of the SiO<sub>2</sub>-NT preparation route.

A faster addition of aqueous ammonia to similar reaction mixture favors the formation of solid spheres instead of nanotubes. Their diameters are about hundreds of nanometers, the samples being denoted as SiO<sub>2</sub>S (S—spheres) (**Figure 4**).

For obtaining thinner (20–50 nm diameter) and longer nanotubes, denoted as SiO<sub>2</sub>Tt (Tt meaning thin tubes) (**Figure 5**), the working temperature decreased at 0°C, and the molar ratio of reactants changed according to the following values: 1 (TEOS):0.03 (tartaric acid):18 (ethanol):10 (H<sub>2</sub>O).

These synthetic conditions allow to obtain not only a better morphological homogeneity than in previous case but also an increased chemical reactivity of the SiO<sub>2</sub> tubular surfaces; their functionalization with NH<sub>2</sub> groups proved to be favored, which is an appropriate functional feature for an efficient inorganic carrier.

The control of the above-described synthesis parameters allows to achieve various and reproducible morphologies. Briefly, the diversity regarding the morphology (spheres and veils) but also the different textural properties of the nanotubes is closely related to the experimental conditions governing both the SiO<sub>2</sub> sol and in situ template generation.

Accordingly, adjustments concerning the SiO<sub>2</sub> sol formation are resulting in appearance of the veil-type morphology (**Figure 6**).

In addition, by using *meso*-tartaric acid instead of DL tartaric acid, small spherical particles (around 40 nm) have been obtained (**Figure 7**).

If DL tartaric acid is replaced by oxalic acid, tubular morphology is maintained. **Figure 8** shows the resulted tubes sized (characterized) at micrometric scale both in diameter and length. These experimental achievements are in line with the literature data [19].

### 3. Modification of SiO<sub>2</sub> tubular matrices with gold nanoparticles

According to literature data, most of the enzymatic immobilization tests on silica are based on electrostatic interactions, resulting in direct adsorption [20, 21]. Gold nanoparticles deposited on silica surface proved to increase the capacity of SiO<sub>2</sub> materials to load the target enzymes [22].

In this sense, gold modification of SiO<sub>2</sub> matrices was performed both by direct impregnation of SiO<sub>2</sub> powder with a solution of HAuCl<sub>4</sub> 3H<sub>2</sub>O and by

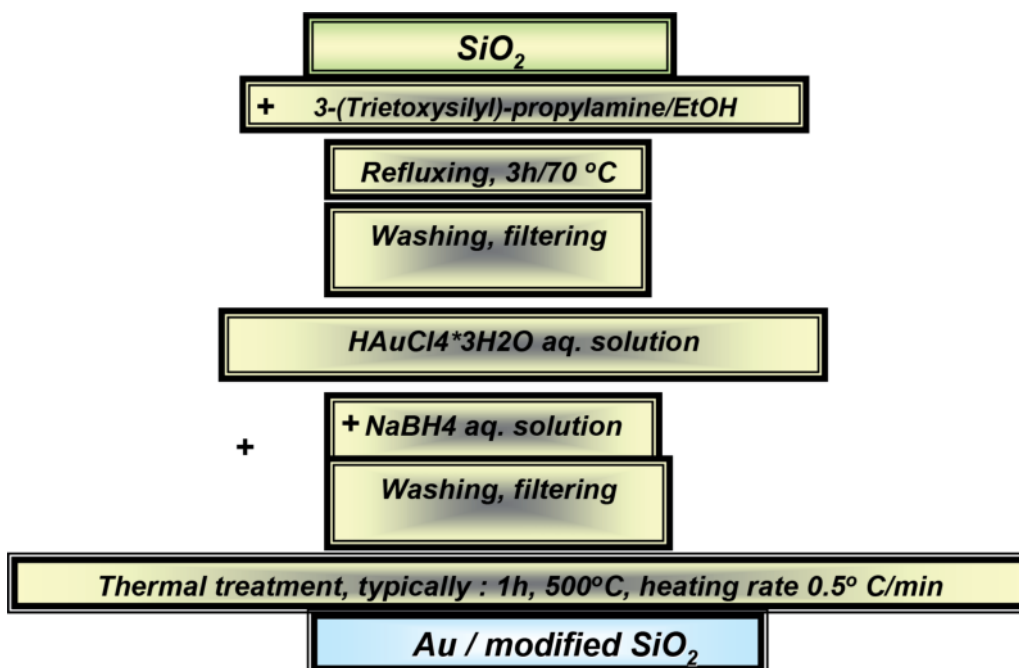


**Figure 2.**  
Schematic representation of the Au-modified SiO<sub>2</sub>-NT preparation route.

deposition of metallic nanoparticles after functionalization of silica surface with 3-(triethoxysilyl)-propylamine.

Direct modification of SiO<sub>2</sub> materials with gold was done using 0.2 g of previously thermally treated SiO<sub>2</sub> (500°C, 3 hours) and an aqueous solution of 0.01 M HAuCl<sub>4</sub> 3H<sub>2</sub>O (49%, Sigma-Aldrich), in order to achieve 2% Au (weight percent). The resulted mixture has been stirred (500 rpm) at room temperature for 5 hours and then calcined 1 h at 300°C with a heating rate of 0.5 deg/min.

The same procedure has been respected for gold modification of SiO<sub>2</sub> surface after functionalization with organic groups (**Figure 2**), which consists in refluxing for 12 hours of a mixture containing 0.2 g SiO<sub>2</sub>, 5 ml absolute ethanol, and 50 microliters (μl) of 3-(triethoxysilyl)-propylamine (C<sub>9</sub>H<sub>23</sub>NO<sub>3</sub>Si, 99%, Sigma-Aldrich).

After washing with ethanol, filtering, and drying, the recovered powder is added to a gold aqueous solution (HAuCl<sub>4</sub> 3H<sub>2</sub>O, 0.01 M) and stirred (500 rpm) at room temperature for 5 hours. An aqueous solution of NaBH<sub>4</sub> (Sigma-Aldrich) is used for reduction of ionic (Au<sup>3+</sup>) to metallic gold, followed by washing, filtering, and calcinations of the recovered product at 500°C for 1 hour, maintaining the same heating rate as for direct impregnation (0.5 deg/min).

The average size of deposited metal nanoparticles evaluated from TEM and X-ray diffraction (XRD) measurements ranged in 5–15 nm domain.

#### 4. Morphological and structural characterization of simple and gold-modified SiO<sub>2</sub>

In order to evaluate the various morphologies displayed by SiO<sub>2</sub> sol-gel materials as a result of ranging the synthetic parameters and to emphasize the fully desired characteristics of SiO<sub>2</sub> matrices for development of hybrid structures with enzymatic activity, scanning and transmission electron microscopies (SEM, TEM), Fourier transform infrared and FTIR-ATR, diffuse reflectance UV-Vis spectroscopy, and XRD measurements were performed.

## 4.1 Characterization of bare SiO<sub>2</sub> materials

### 4.1.1 Scanning and transmission electron microscopy (SEM and TEM)

SEM investigations (**Figure 3**, for the SiO<sub>2</sub>TL sample) clearly show the tubular morphology as major phase of the SiO<sub>2</sub> powders resulted from the sol-gel process.

SEM images from **Figure 3a–d** reveal a small percent of rounded particles, most of them being attached to the external surface of the tubes. This observation is in line with reported literature data about SiO<sub>2</sub> tubular matrices obtained in mild conditions, by sol-gel process [18]. Their average external diameter is around 200 nm, the length overcoming 1 μm. An accurate perspective on the wall structure of these large nanotubes (SiO<sub>2</sub>TL) is achieved by TEM images from **Figure 3e, f**. So, thick walls with porous structure, empty core, and open ends of the nanotubes could be observed.

**Figure 4** shows the presence of solid, big spheres with an average diameter of 200 nm, no other morphologies being present.

**Figure 5** presents thin nanotubes (SiO<sub>2</sub>Tt) (average diameter ~50 nm) like predominant morphology, spherical entities being present on their surface but as smaller percent than for the previous tubular sample (SiO<sub>2</sub>TL). From this point of view, it is obvious that the sample has a high degree of homogeneity. Also, the tubes

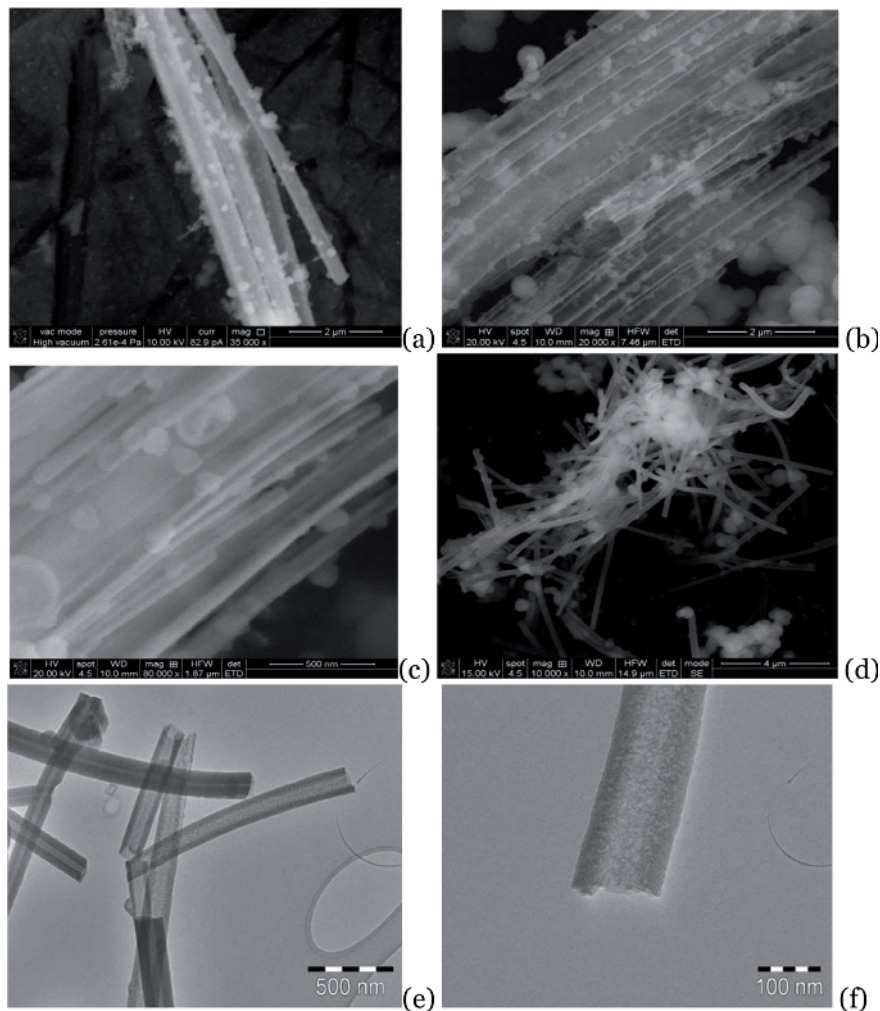


**Figure 3.** (a–d) SEM images at different magnifications of large tubes (SiO<sub>2</sub>TL)—unpublished results; (e, f) TEM images of large tubes (SiO<sub>2</sub>TL). (e, f) (Reprinted from [7] with permission from Elsevier).

are thinner and much longer than previous ones, the ratio between the external and internal diameters being also decreased. Despite their impressive length, similar to that of the fibers, the SEM images captured at 1  $\mu\text{m}$  scale bar show a good contrast between their walls and empty cores. This means high surface (both internal and external) areas are available for interaction (contact) with enzymes. In addition to BET results, these images indicate a facile access but also a potential confinement [23] of the enzymes inside the tubes which could favor an increased degree of enzymatic immobilization.

**Figure 6** presents images of a single and distinct morphology obtained by sol-gel method, namely,  $\text{SiO}_2$  veils. In addition to the previously reported application, as support and part in composite structures [11], many potential applications could exploit the lack of toxicity but especially the great structural and morphological homogeneity of this  $\text{SiO}_2$  matrix, especially in biomaterial range.

**Figures 7 and 8** are also relevant for the influence of the synthesis parameters on the morphological features of the synthesized material. The change of the organic template leads to rounded, quite undefined nanoparticles characterized by the SEM images from **Figure 7** and the modified tubular morphology being exposed in **Figure 8**. These images are recorded for a sample whose characteristics have been tailored by the oxalic acid used as template. Huge tubes can be observed and enlarged especially as diameters (up to 5  $\mu\text{m}$ ).

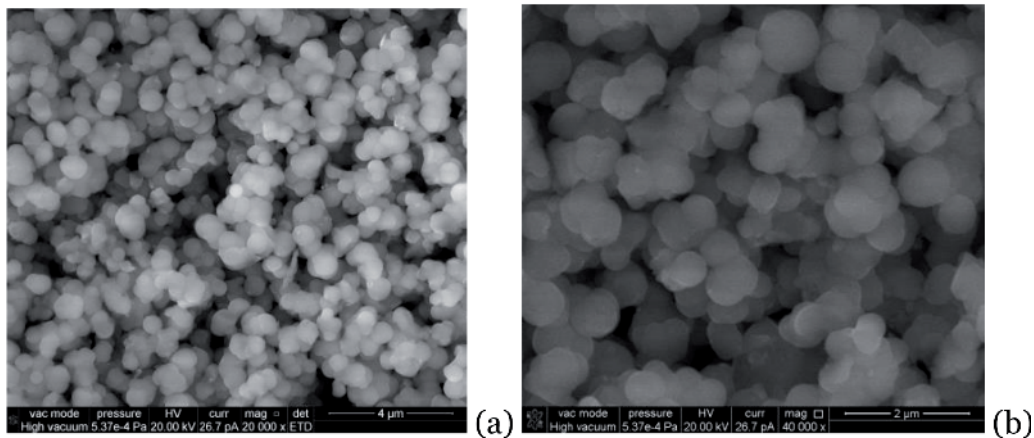


**Figure 4.**  
SEM images of  $\text{SiO}_2$  spheres ( $\text{SiO}_2\text{S}$ ). (Reprinted from [17]).

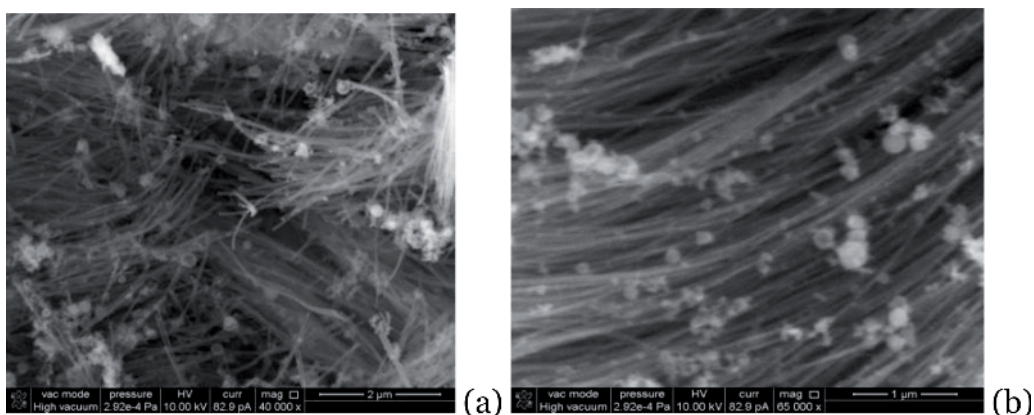


**Figure 5.**  
SEM images of thin tubes ( $\text{SiO}_2\text{Tt}$ ). (Reprinted from [17]).

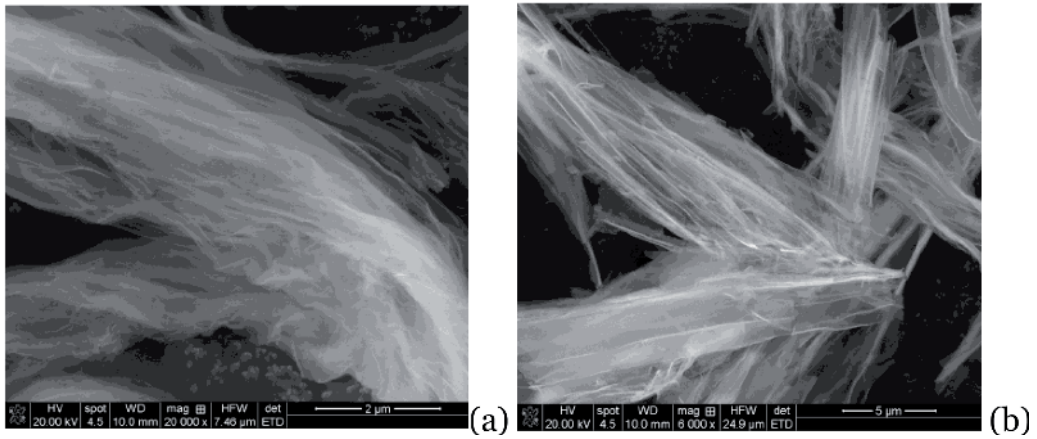


**Figure 6.**  
SEM images of sol-gel SiO<sub>2</sub> veils (SiO<sub>2</sub>.v). (Unpublished results).

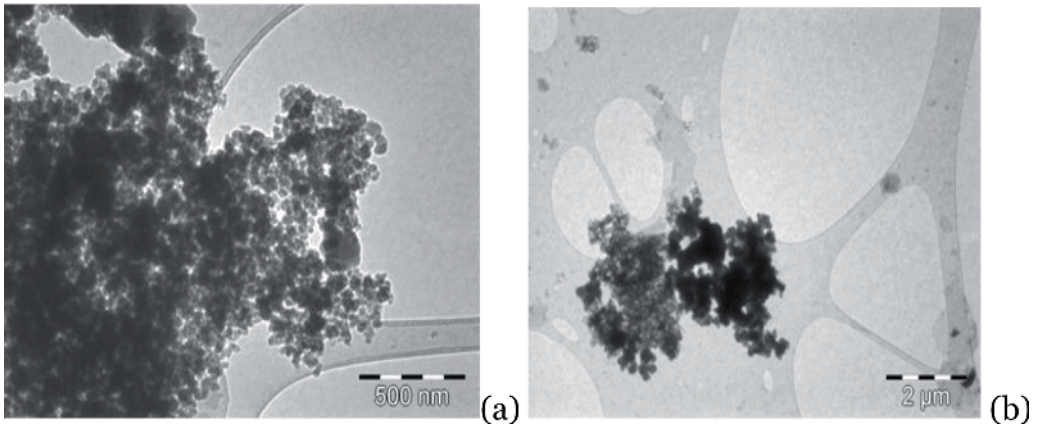


**Figure 7.**  
TEM images of spherical SiO<sub>2</sub> nanoparticles (SiO<sub>2</sub>.s). (Reprinted from [7] with permission from Elsevier).

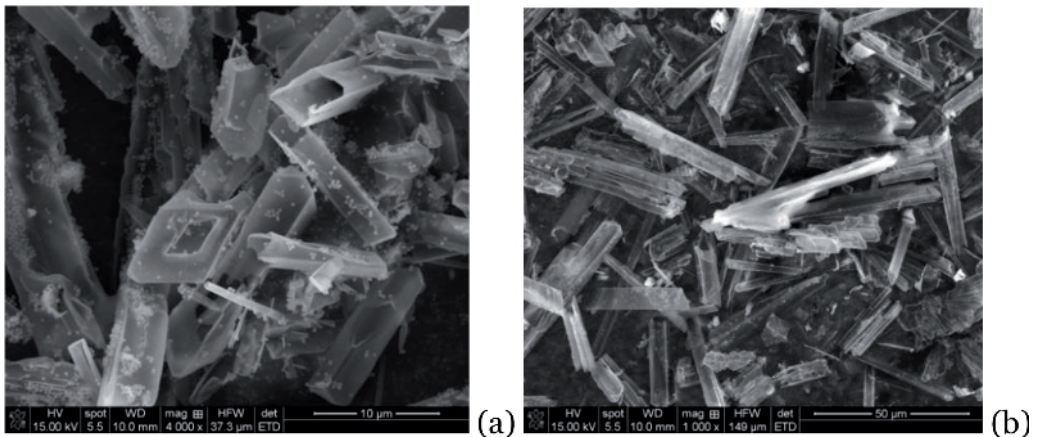


**Figure 8.**  
SEM images of extra large SiO<sub>2</sub> tubes (SiO<sub>2</sub>.TXL) obtained with oxalic acid as template. (Unpublished results).

#### 4.1.2 Fourier transform infrared spectroscopy (FTIR)

Taking into account the target application for these SiO<sub>2</sub>-based materials, namely, the immobilization of enzymes, the information obtained by FTIR

regarding the structural characteristics of SiO<sub>2</sub> inorganic matrix and its interaction with functional organic groups are useful.

The relevant vibration bands observed from FTIR spectra of the spherical and tubular SiO<sub>2</sub> samples (**Figure 9**) are similar; small variations could be perceived especially regarding their intensity and the presence of silanol groups (Si-OH), which is an important issue from the perspective of further functionalization of silica surface with 3-(triethoxysilyl)-propylamine (APTES) and, subsequently, the deposition of gold on the surface.

According to our previous collected results and literature data, the large peak from 1124 cm<sup>-1</sup> is due to Si-O stretching from SiO<sub>2</sub> [7], and its shoulder (1200 cm<sup>-1</sup>) is assigned to asymmetric vibration of Si-O-Si [24]. One more tiny shoulder located around ~960 cm<sup>-1</sup> could indicate the presence of silanol groups [25], especially for spherical SiO<sub>2</sub> (SiO<sub>2</sub>S) but unperceivable for the sample containing large tubes (SiO<sub>2</sub>TL). Its spectrum indicates also less structural, free OH groups and adsorbed water, generally evaluated from the development of a broadband ranging in 3350–3600 cm<sup>-1</sup> domain [26, 27]. The presence of OH groups on silica surface could promote the hydrogen bonding formation with functional groups of enzymes [28]. According to the reported data [8], the peak located at 847 cm<sup>-1</sup> is due to  $\nu_{s(\text{Si-O-Si})}$ , and the peak appearing to 484 cm<sup>-1</sup> is determined by  $\delta_{(\text{Si-O-Si})}$ .

In order to identify and characterize gold nanoparticles deposited on the surface of thin tubes by direct impregnation of powder with gold precursor solution, SEM analysis (**Figure 10a**) was performed. A very large size distribution associated with a weak dispersion of gold nanoparticles could be observed.

In the case of gold deposition after surface functionalization with APTES, smaller gold nanoparticles were expected to result. **Figure 11a** presents a SEM image of the metal-modified nanotubes, but gold nanoparticles are unperceivable because of their reduced dimensions as a result of previous surface functionalization. Accordingly, TEM analysis was performed, and the images from **Figure 11b** show smaller gold nanoparticles with average diameter around 7 nm, deposited on external surface of nanotubes which bear as well spherical particles of SiO<sub>2</sub>. Also, a loss of transparency could be observed in the case of functionalized samples. Images from **Figures 10** and **11** emphasize more efficient gold deposition after functionalization of SiO<sub>2</sub> tubular surface, exhibiting small, well-dispersed gold nanoparticles which should successfully bind the enzymes.

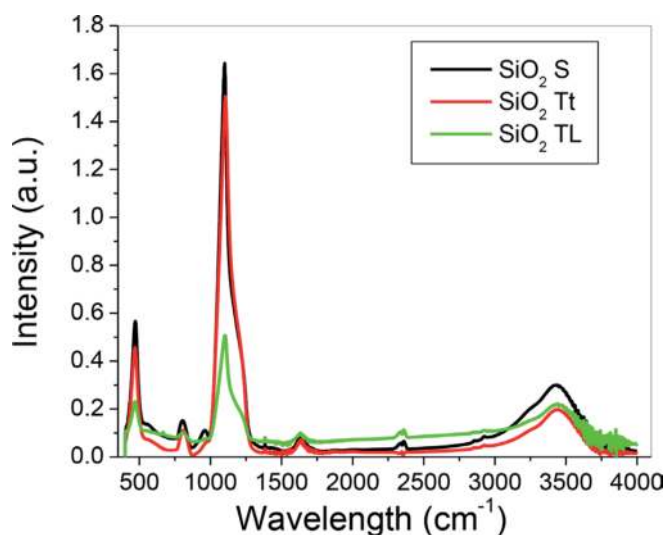


**Figure 9.** FTIR spectra of SiO<sub>2</sub> spheres (SiO<sub>2</sub>S), SiO<sub>2</sub> thin tubes (SiO<sub>2</sub>Tt), and SiO<sub>2</sub> large tubes (SiO<sub>2</sub>TL).



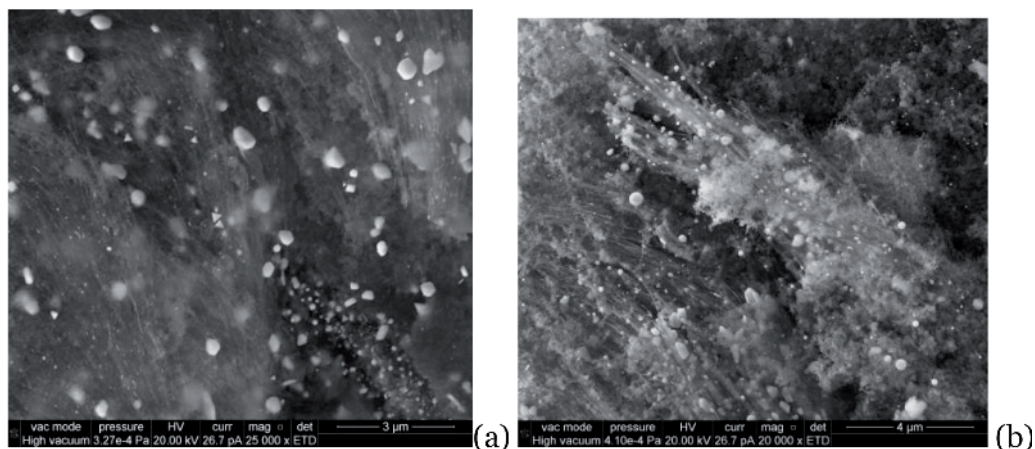


**Figure 10.** SEM images of gold-modified silica thin tubes, by direct impregnation (AuSiO<sub>2</sub>Tt). (Unpublished results).

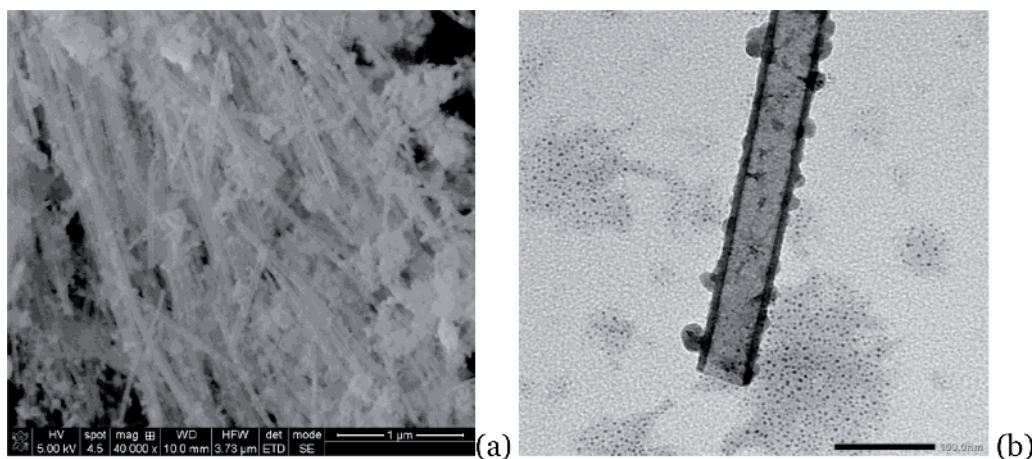


**Figure 11.** (a) SEM images of SiO<sub>2</sub> thin tubes modified with gold after functionalization with APTES (AuSiO<sub>2</sub>TtF). (b) TEM images of SiO<sub>2</sub> thin tubes modified with gold after functionalization with APTES (AuSiO<sub>2</sub>TtF). (Unpublished results).

#### 4.1.3 Diffuse reflectance UV-Vis spectroscopy performed on silica and gold-modified silica thin tubes

The main objective of this investigation was to observe the surface plasmon resonance (SPR) phenomenon which is related to gold nanoparticles contained by the analyzed samples. As it could be seen from **Figure 12**, a large peak appears around 500 nm for the gold-modified SiO<sub>2</sub> samples, this being more impressive when gold is deposited after functionalization of SiO<sub>2</sub> thin tubes (AuSiO<sub>2</sub>TtF).

#### 4.1.4 X-ray diffraction (XRD)

The XRD results are presented in **Figure 13**, where the broad diffraction band located at  $2\theta = 21.5^\circ$  is characteristic to the amorphous structure of SiO<sub>2</sub> and the maxima from  $2\theta = 38.17, 44.3, 64.5, 77.5^\circ$  are typical for metallic gold. The average crystallite size of the gold deposited after functionalization of silica surface, calculated with Williamson-Hall method, is 7.5 nm, much smaller than for the other sample (~ 15 nm).

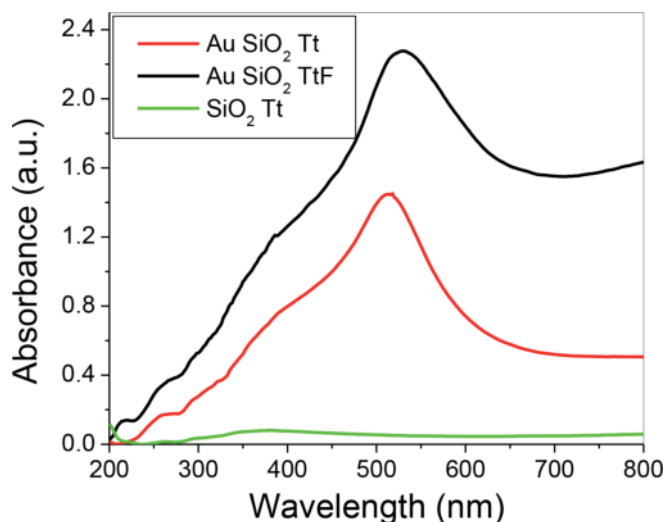


**Figure 12.**

UV-Vis spectra of silica and gold-modified silica tubes by direct impregnation ( $AuSiO_2Tt$ ) and after functionalization ( $AuSiO_2TtF$ ). (Unpublished results).

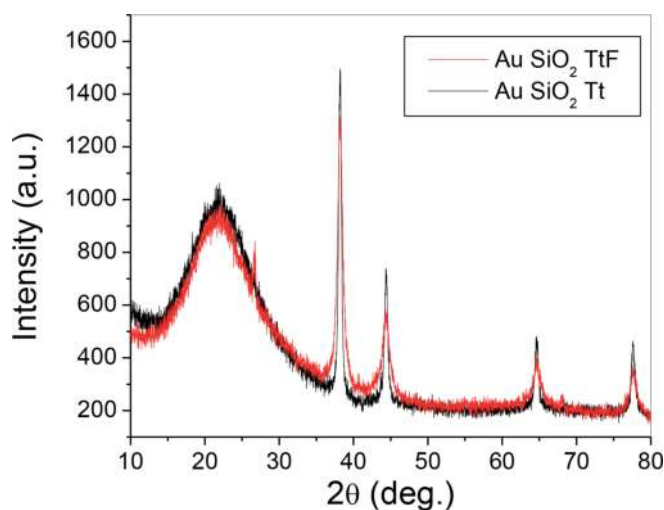


**Figure 13.**

XRD spectra of gold-modified silica thin tubes by direct impregnation ( $AuSiO_2Tt$ ) and after functionalization ( $AuSiO_2TtF$ ). (Unpublished results).

#### 4.1.5 Fourier transform infrared spectroscopy (FTIR)

Analysis of spectra from **Figures 15** and **16** (details of general spectrum from **Figure 14**) shows that after silica thin tube functionalization, its spectra do not present the specific vibrations of Si-OH ( $\sim 960\text{ cm}^{-1}$ ), free or bounded OH groups, and adsorbed water ( $3350\text{--}3600\text{ cm}^{-1}$ ). This supports the idea that 3-(triethoxysilyl)-propylamine is anchored by the OH groups of the tubular silica surface.

#### 4.1.6 FTIR-ATR spectroscopy performed on functionalized (APTES) $SiO_2$ thin tubes

FTIR-ATR measurements were done in order to check the functionalization of  $SiO_2Tt$  surface with functional groups of 3-(triethoxysilyl)-propylamine.

**Figure 17** identifies the peak located at 1635 cm<sup>-1</sup> which, according to the literature data, is attributed to the twisting vibration of N-H in addition to the band from 3000 to 2900 cm<sup>-1</sup> due to the stretching vibration of the CH<sub>2</sub> which proves the successful functionalization of silica with APTES [29, 30].

It is obvious from **Figure 18** that the chemical “fingerprint” of the SiO<sub>2</sub> inorganic matrix is preserved, but the organic groups identified in previous spectrum are strongly flattened, due to the thermal treatment applied after functionalization and gold modification, respectively. As expected, the broadband (3400–3600 cm<sup>-1</sup>) related to OH groups and adsorbed water is clearly diminished, as well as the band from 2900 to 3000 cm<sup>-1</sup> (the stretching vibration due to CH<sub>2</sub> from APTES).

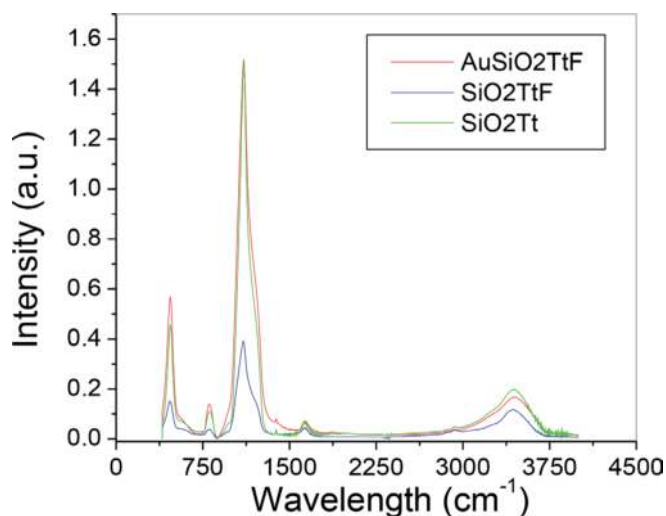


**Figure 14.** General FTIR spectra of simple, functionalized, and gold-modified SiO<sub>2</sub> thin tubes: SiO<sub>2</sub> (SiO<sub>2</sub>Tt), SiO<sub>2</sub>-APTES (SiO<sub>2</sub>TtF), and AuSiO<sub>2</sub>-APTES (AuSiO<sub>2</sub>TtF). (Unpublished results).

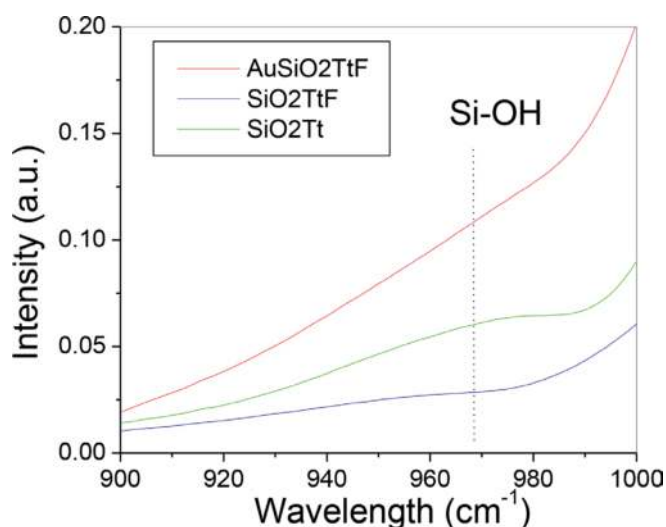


**Figure 15.** FTIR spectra of simple, functionalized, and gold-modified SiO<sub>2</sub> thin tubes: SiO<sub>2</sub> (SiO<sub>2</sub>Tt), SiO<sub>2</sub>-APTES (SiO<sub>2</sub>TtF), and AuSiO<sub>2</sub>-APTES (AuSiO<sub>2</sub>TtF) in 900–1000 cm<sup>-1</sup> region. (Unpublished results).

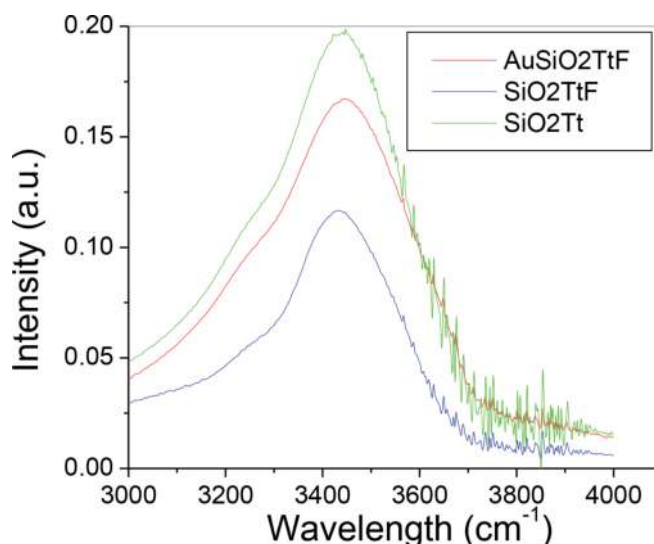


**Figure 16.** FTIR spectra of simple, functionalized, and gold-modified  $\text{SiO}_2$  thin tubes:  $\text{SiO}_2$  ( $\text{SiO}_2\text{Tt}$ ),  $\text{SiO}_2$ -APTES ( $\text{SiO}_2\text{TtF}$ ), and  $\text{AuSiO}_2$ -APTES ( $\text{AuSiO}_2\text{TtF}$ ) in  $3000\text{--}4000\text{ cm}^{-1}$  region. (Unpublished results).

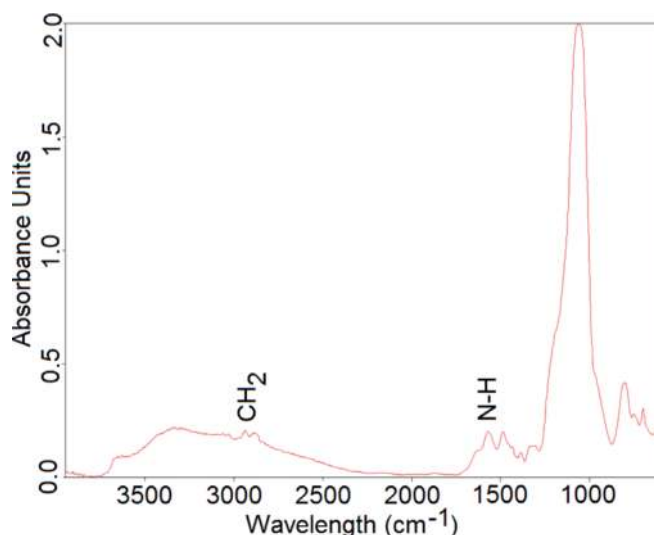


**Figure 17.** FTIR-ATR spectrum of thin tubes ( $\text{SiO}_2\text{TtF}$ ) functionalized with 3-(triethoxysilyl)-propylamine. (Unpublished results).

## 5. Synthesis, characterization, and catalytic activity of hybrid complex lipase-inorganic matrices ( $\text{SiO}_2$ , $\text{AuSiO}_2\text{Tt}$ )

### 5.1 Synthesis of lipase- $\text{SiO}_2$ complex

Generally, the design of hybrid structures like enzyme-inorganic carrier is looking to preserve or increase the catalytic activity of free enzymes but especially to extend its lifetime and endurance in relation to parameters governing its proximity (pH, temperature) [31]. In addition to this, enzymatic immobilizations have the advantage of reusability which is an important issue especially for those biocatalysts meant to sustain valuable biotechnologies. For instance, free and immobilized

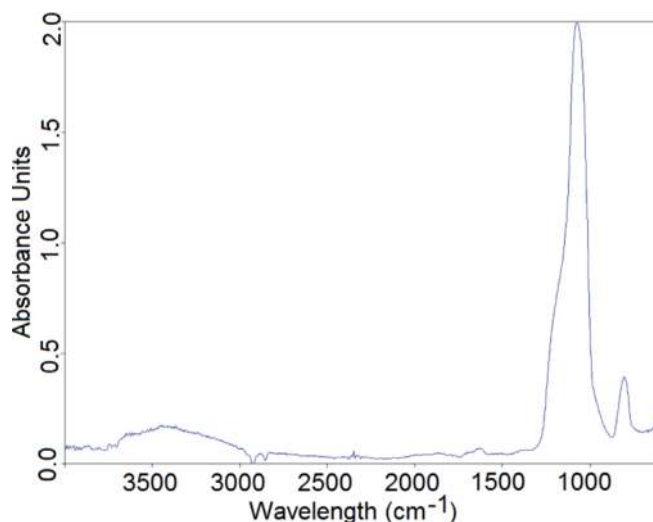


**Figure 18.** FTIR-ATR spectrum of gold-modified thin tubes ( $AuSiO_2TtF$ ) after functionalization with 3-(triethoxysilyl)propylamine. (Unpublished results).

lipase is used in esterification, transesterification, reactions [32, 33], and different biotechnological applications [34].

According to literature data, gold nanoparticles could increase the enzyme loading on inorganic carriers, acting as efficient support for enzymes [35]. Few but important potential medical applications are centered on the use of lipase immobilized on gold nanoparticles as electrochemical sensor for triglycerides from human serum [36].

The literature results indicate the isoelectric point of lipase from *Rhizopus oryzae* and silica at pH 7.6 and 3, respectively [21]. In order to achieve an electrostatic attraction between SiO<sub>2</sub> supports and lipase, our immobilization experiments were conducted at pH 6.3 where lipase is slightly positively charged.

Briefly, hybrid complex material consisting in lipase-inorganic support (SiO<sub>2</sub>Tt, AuSiO<sub>2</sub>Tt) was obtained according to the previous reported work [17] concerning the generation of biocatalyst lipase-SiO<sub>2</sub> matrices. Lipase (*Rhizopus oryzae*, Sigma-Aldrich) in phosphate buffer (pH 6.3) was mixed with SiO<sub>2</sub> and Au/SiO<sub>2</sub> powder (0.02 g) also dispersed in phosphate buffer and magnetically stirred 24 h (100°C). The solid product containing lipase immobilized on SiO<sub>2</sub> and Au/SiO<sub>2</sub> powder was separated from supernatant by centrifugation and washed several times with phosphate buffer and water in order to be further evaluated from the perspective of total organic carbon content, FTIR-ATR and PZC measurements, and enzymatic tests as well.

## 5.2 Characterization of lipase-SiO<sub>2</sub> complex

### 5.2.1 BET measurements

The textural properties of tubular and spherical silica, correlated with total organic carbon measurement on their lipase derivative hybrid complex, were previously evaluated and reported [17].

Accordingly, a surface area ( $S_{BET}$ ) about 18 and 14m<sup>2</sup>/g, respectively, was found for large tubes (SiO<sub>2</sub>TL) and spherical (SiO<sub>2</sub>S) samples. In the case of large tubes,

mesopores of 3 nm were identified, which are probably located in the walls of the nanotubes but improper for the lipase immobilization (the diameter of *Rhizopus oryzae* being  $\sim 5$  nm). SEM and TEM images (Figure 3) show an internal diameter of  $\sim 200$  nm, and total organic carbon measurements [17] indicate the best lipase loading on SiO<sub>2</sub>Tt sample (30 mg/g). It is obvious that the internal surfaces are accessible for lipase immobilization.

Spherical SiO<sub>2</sub> matrices (SiO<sub>2</sub>S) show a large size distribution of pores, ranging from 3 to 5 nm and from 10 to 30 nm. Probably, the last value is due to voids of packed spheres and could hardly allow the enzymatic immobilization, but leaching could be favored too.

Figure 19 presents the data related to SiO<sub>2</sub> tubular thin tube sample (SiO<sub>2</sub>Tt).

From BET analysis, the value of the specific surface area ( $S_{\text{BET}}$ ) was found to be 107.83 m<sup>2</sup>/g. The shape of adsorption and desorption branches is typical for cylindrical pores with open ends. The pore size distribution is very large, spanning from 10 to 100 nm. By correlating these results with SEM images (Figure 5), it can be assumed that the internal diameters of these thin tubes are ranging between 10 and 50 nm. The well-defined peak from 3 nm can be attributed to the mesoporosity of wall nanotubes, similar to larger ones (SiO<sub>2</sub>TL). These properties are drastically changed by the lipase adsorption; the broad peak ranging between 10 and 100 nm is not present anymore. This proves that the immobilization of lipase on SiO<sub>2</sub>Tt sample is in fact a confinement inside the core of the nanotubes which can assure an increased stability against post-immobilization leaching. Total organic carbon analysis sets the capacity of loading the lipase around 15 mg/g, lower than for larger tubes but better than for spherical ones.

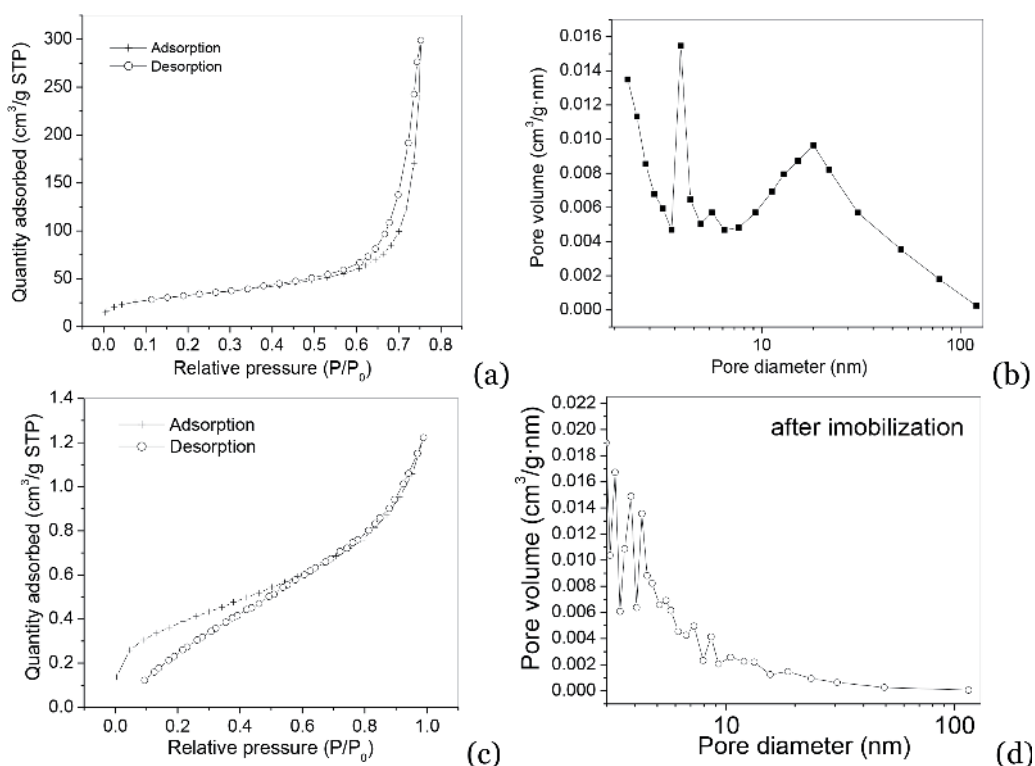


**Figure 19.**

*N*<sub>2</sub> adsorption-desorption isotherms (a) and the pore size distribution obtained from the desorption branch (b) for the SiO<sub>2</sub>Tt samples before lipase immobilization; (c and d) the same curves recorded after lipase immobilization. (Reprinted from [17]).

### 5.2.2 FTIR-ATR measurements

Our reported data containing the FTIR-ATR results registered on lipase-SiO<sub>2</sub> hybrid complex [17] indicated the presence of lipase and its specific vibration bands both in supernatant and onto solid tubular and spherical SiO<sub>2</sub> supports (**Figure 20**).

The previous reported capacity of unmodified SiO<sub>2</sub> matrices to load lipase was found to fit to the following sequence: SiO<sub>2</sub>TL > SiO<sub>2</sub>Tt > SiO<sub>2</sub>S (**Figure 20a**).

The comparison of **Figure 20a, b** highlights especially the peak from 3271 cm<sup>-1</sup> (marking the stretching vibration of the NH group). In this sense, it appears that lipase from supernatant solution (of the derivative hybrid complex of gold-modified SiO<sub>2</sub>Tt) is less emphasized. This observation means a higher capacity of gold-modified sample to uptake lipase than the bare SiO<sub>2</sub>Tt carrier. Thus, the gold modification of silica looks to be successful and worth to be further investigated.

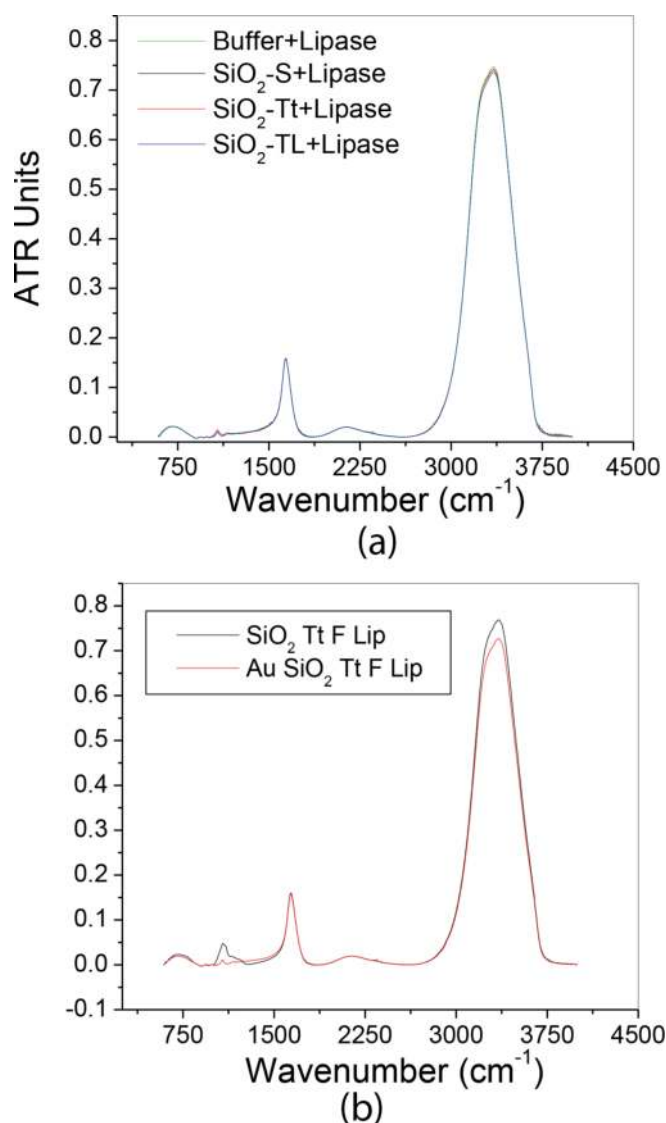


**Figure 20.** (a) FTIR-ATR spectra recorded from supernatant solution after immobilization of lipase on different SiO<sub>2</sub> samples in phosphate buffer solution, revealing the 3271 cm<sup>-1</sup> peak. (Reprinted from [17]); (b) FTIR-ATR spectra recorded from supernatant solution after immobilization of lipase on SiO<sub>2</sub>Tt and AuSiO<sub>2</sub>Tt supports. (Unpublished results).

### 5.2.3 The electrokinetic potential

The electrokinetic potential ( $\xi$ ) measurements (**Figure 21**) bring information related to the electrostatic interactions established between the surfaces of inorganic carrier and enzyme, which is actually a decisive parameter for an efficient enzymatic immobilization by direct adsorption.

The lipase immobilization on  $\text{SiO}_2$  and gold-modified  $\text{SiO}_2$  matrices was performed at pH 6.3 in phosphate buffer solution. In these conditions, the silica should be negatively charged and lipase slightly positive. Our previous results [17] indicate highly negative values of electrokinetic potential ( $\xi$ ), especially for spherical samples. After immobilization (**Figure 21a**), these values slightly change, probably due to the lipase adsorption on the external surface of  $\text{SiO}_2$  matrices. From the above-presented data, the immobilization of lipase on  $\text{SiO}_2\text{Tt}$  sample takes place especially inside the nanotubes.

**Figure 21b** displays the values of electrokinetic potential ( $\xi$ ) for gold-modified thin nanotubes, both by direct impregnation ( $\text{AuSiO}_2\text{Tt}$ ) and after

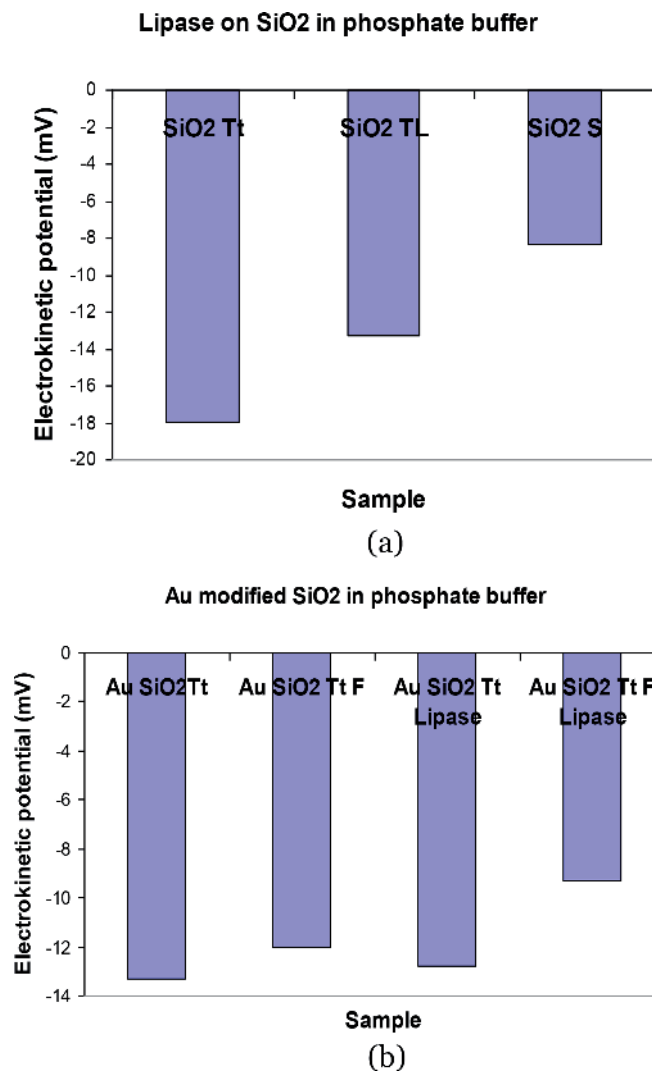


**Figure 21.**

(a) The electrokinetic potential of lipase-bare  $\text{SiO}_2$  hybrid systems. (Adapted from [17]); (b) Gold-modified  $\text{SiO}_2\text{Tt}$  together with developed lipase hybrid complex. (Unpublished results).



functionalization with APTES (AuSiO<sub>2</sub>TtF), before and after lipase immobilization. It is obvious that the deposition of gold after surface functionalization is more efficient in terms of the inorganic host ability to immobilize the lipase, this fact being illustrated in **Figure 21b** as a shift of the electrokinetic potential ( $\xi$ ) to more positive values.

### 5.3 Catalytic activity of lipase-SiO<sub>2</sub> complex

Our previously reported data [17] are concerning the catalytic activity of lipase from *Rhizopus oryzae* immobilized on bare tubular and spherical SiO<sub>2</sub> matrices for hydrolysis reaction of p-nitrophenyl acetate (p-NPA).

Briefly, the hybrid complex newly formed is suspended in dimethyl sulfoxide (DMSO) and phosphate buffer at pH 7.8. One hour of incubation at 37°C is allowed, and the liquid phase was separated by centrifugation for measuring the reaction products by UV-Vis.

The best biocatalyst in terms of highest product amount (p-nitrophenyl) proved to result from lipase immobilization on SiO<sub>2</sub> thin tubes. For this reason, gold nanoparticle modification of this inorganic matrix should result in optimization of structural and functional properties of its derivative hybrid complex with lipase. This aspect was addressed by the above-presented structural characterization of gold-modified SiO<sub>2</sub>Tt support, and its derivative complex and further investigations regarding their enzymatic activity will be performed.

## 6. Conclusions

Sol-gel method proves to be an efficient tool for obtaining well-defined SiO<sub>2</sub>-based multifunctional materials (bio-/photocatalysis, bioremediation processes, electrochemistry).

SiO<sub>2</sub> inorganic carriers obtained by in situ generated template-assisted sol-gel method revealed morphology-dependent behavior regarding lipase (*Rhizopus oryzae*) immobilization and enzymatic activity of the derivative hybrid complex.

Gold modification of functionalized (APTES) SiO<sub>2</sub> tubular surfaces improves the degree of enzymatic immobilization.

## Conflict of interest

The authors declare no conflict of interest.


## **Author details**

Crina Anastasescu, Mihai Anastasescu, Ioan Balint and Maria Zaharescu\*  
“Ilie Murgulescu” Institute of Physical Chemistry of the Romanian Academy,  
Bucharest, Romania

\*Address all correspondence to: [mzaharescu@icf.ro](mailto:mzaharescu@icf.ro)

## **IntechOpen**

---

© 2019 The Author(s). Licensee IntechOpen. This chapter is distributed under the terms of the Creative Commons Attribution License (<http://creativecommons.org/licenses/by/3.0>), which permits unrestricted use, distribution, and reproduction in any medium, provided the original work is properly cited. 

## References

- [1] Shiraishi F, Toyoda K, Fukinbara S, Obuchi E, Nakano K. Photolytic and photocatalytic treatment of an aqueous solution containing microbial cells and organic compounds in an annular-flow reactor. *Chemical Engineering Science*. 1999;**54**(10):1547-1552. DOI: 10.1016/S0009-2509(99)00068-8
- [2] Parvulescu V, Dascalescu C, Su BL. Highly selective oxidation of styrene with hydrogen peroxide catalyzed by mono- and bimetallic (Ni, Ni-Cr and Ni-Ru) incorporated MCM-41 silicas. *Studies in Surface Science and Catalysis*. 2003;**146**:629-632. DOI: 10.1016/S0167-2991(03)80462-7
- [3] Nassif N, Bouvet O, Rager MN, Roux C, Coradin T, Livage J. Living bacteria in silica gels. *Nature Materials*. 2002;**1**:42-44. DOI: 10.1038/nmat709
- [4] Mondal S, Malik S, Sarkar R, Roy D, Saha S, Mishra S, et al. Exuberant immobilization of urease on an inorganic support SiO<sub>2</sub> enhancing the enzymatic activities by threefold for perennial utilization. *Bioconjugate Chemistry*. 2019;**30**(1):134-147. DOI: 10.1021/acs.bioconjchem.8b00796
- [5] Jiang Y, Wang W, Li X, Wang X, Zhou J, Mu X. Enzyme-mimetic catalyst-modified nanoporous SiO<sub>2</sub>-cellulose hybrid composites with high specific surface area for rapid H<sub>2</sub>O<sub>2</sub> detection. *ACS Applied Materials and Interfaces*. 2013;**5**(6):1913-1916. DOI: 10.1021/am400253d
- [6] Kadam AA, Yang J, Lee DS. Supermagnetically tuned halloysite nanotubes functionalized with aminosilane for covalent laccase immobilization. *ACS Applied Materials & Interfaces*. 2017;**9**(18):15492-15501. DOI: 10.1021/acsami.7b02531
- [7] Anastasescu C, Anastasescu M, Teodorescu VS, Gartner M, Zaharescu M. SiO<sub>2</sub> nanospheres and tubes obtained by sol-gel method. *Journal of Non-Crystalline Solids*. 2010;**356**:2634-2640. DOI: 10.1016/j.jnoncrysol.2010.03.038
- [8] Anastasescu C, Mihaiu S, Preda S, Zaharescu M. 1D Oxide Nanostructures Obtained by Sol-Gel and Hydrothermal Methods. Cham, Switzerland: Springer; 2016. ISBN 978-3-319-32988-8
- [9] Anastasescu C, Anastasescu M, Zaharescu M, Balint I. Platinum-modified SiO<sub>2</sub> with tubular morphology as efficient membrane-type microreactors for mineralization of formic acid. *Journal of Nanoparticle Research*. 2012;**14**:1198. DOI: 10.1007/s11051-012-1198-5
- [10] Anastasescu C, Zaharescu M, Balint I. Unexpected photocatalytic activity of simple and platinum modified tubular SiO<sub>2</sub> for the oxidation of oxalic acid to CO<sub>2</sub>. *Catalysis Letters*. 2009;**132**:81-86. DOI: 10.1007/s10562-009-0066-0
- [11] Spătaru T, Kondo T, Anastasescu C, Balint I, Osiceanu P, Munteanu C, et al. Silica veils-conductive diamond powder composite as a new propitious substrate for platinum electrocatalysts. *Journal of Solid State Electrochemistry*. 2017;**21**(4):1007-1014. DOI: 10.1007/s10008-016-3454-6
- [12] Anastasescu C, Zaharescu M, Angelescu D, Munteanu C, Bratan V, Spataru T, et al. Defect-related light absorption, photoluminescence and photocatalytic activity of SiO<sub>2</sub> with tubular morphology. *Solar Energy Materials and Solar Cells*. 2017;**159**:325-335. DOI: 10.1016/j.solmat.2016.09.032
- [13] Spataru N, Anastasescu C, Radu MM, Balint I, Spataru T, Fujishima A. The improvement of SiO<sub>2</sub> nanotubes electrochemical behavior by hydrogen

- atmosphere thermal treatment. *Applied Surface Science*. 2018;**444**:216-223. DOI: 10.1016/j.apsusc.2018.03.074
- [14] Anastasescu C, Negrila C, Angelescu DG, Atkinson I, Anastasescu M, Spataru N, et al. Particularities of photocatalysis and formation of reactive oxygen species on insulators and semiconductors: Cases of SiO<sub>2</sub>, TiO<sub>2</sub> and their composite SiO<sub>2</sub>-TiO<sub>2</sub>. *Catalysis Science & Technology*. 2018;**8**: 5657-5668. DOI: 10.1039/C8CY00991K
- [15] Enache M, Neagu S, Anastasescu C, Cojoc R, Zaharescu M. The effects of silica nanostructures on halotolerant microorganisms isolated from rock salt crystal. *New applications of nanomaterials*, series In: Dascălu D, Cârjă G, Ciurea ML, Catrinel Ion A, editors. *Micro and Nanoengineering*. Ed Acad Rom, Bucharest: Romania; 2014. pp. 51-59
- [16] Neagu S, Preda S, Anastasescu C, Zaharescu M, Enache M, Cojoc R. The functionalization of silica and titanate nanostructures with halotolerant proteases. *Revue Roumaine de Chimie*. 2014;**59**(2):97-103
- [17] Anastasescu C, Preda S, Rusu A, Culita D, Plavan G, Strungaru S, et al. Tubular and spherical SiO<sub>2</sub> obtained by sol-gel method for lipase immobilization and enzymatic activity. *Molecules*. 2018;**23**:1362. DOI: 10.3390/molecules23061362
- [18] Nakamura H, Matsui Y. Silica gel nanotubes obtained by the sol-gel method. *Journal of the American Chemical Society*. 1995;**117**:2651-2652. DOI: 10.1021/ja00114a031
- [19] Miyaji F, Davis SA, Charmant JPH, Mann S. Organic crystal templating of hollow silica fibers. *Chemistry of Materials*. 1999;**11**(11):3021-3024. DOI: 10.1021/cm990449v
- [20] Bai Y, Yang H, Yang W, Li Y, Sun C. Gold nanoparticles-mesoporous silica composite used as an enzyme immobilization matrix for amperometric glucose biosensor construction. *Sensors and Actuators B*. 2007;**124**:179-186. DOI: 10.1016/j.snb.2006.12.020
- [21] Gustafsson H, Johansson EM, Barrabino A, Odén M, Holmberg K. Immobilization of lipase from *Mucor miehei* and *Rhizopus oryzae* into mesoporous silica - the effect of varied particle size and morphology. *Colloids and Surfaces B: Biointerfaces*. 2012;**100**:22-30. DOI: 10.1016/j.colsurfb.2012.04.042
- [22] Mukhopadhyay K, Phadtare S, Vinod VP, Kumar A, Rao M, Chaudhari RV, et al. Gold nanoparticles assembled on amine-functionalized Na-Y zeolite: A biocompatible surface for enzyme immobilization. *Langmuir*. 2003;**19**(9):3858-3863. DOI: 10.1021/la0268202
- [23] Nguyen DT, Smit M, Dunn B, Zink JI. Stabilization of creatine kinase encapsulated in silicate sol-gel materials and unusual temperature effects on its activity. *Chemistry of Materials*. 2002;**14**:4300-4306. DOI: 10.1021/cm020398t
- [24] Ruscher CH, Bannat I, Feldhoff A, Ren L, Wark M. SiO<sub>2</sub> nanotubes with nanodispersed Pt in the walls. *Microporous and Mesoporous Materials*. 2007;**99**:30-36. DOI: 10.1016/j.micromeso.2006.07.032
- [25] Lopez T, Romero A, Gomez R. Metal-support interaction in Pt/SiO<sub>2</sub> catalysts prepared by sol-gel method. *Journal of Non-Crystalline Solids*. 1991;**127**:105-113. DOI: 10.1016/0022-3093(91)90406-V
- [26] Bey Temsamani M, Maeck M, El Hassani I, Hurwitz HD. Fourier transform infrared investigation of water states in Aerosol-OT reverse micelles as a function of counterionic

- nature. *The Journal of Physical Chemistry. B.* 1998;**102**:3335-3340. DOI: 10.1021/jp971844g
- [27] Pickup DM, Mountjoy G, Wallidge GW, Anderson R, Cole JM, Newport RJ, et al. A structural study of (TiO<sub>2</sub>)<sub>x</sub>(SiO<sub>2</sub>)<sub>1-x</sub> (x=0.18, 0.30 and 0.41) xerogels prepared using acetylacetone. *Journal of Materials Chemistry.* 1999;**9**:1299-1305. DOI: 10.1039/a809810g
- [28] Gustafsson H, Thorn C, Holmberg K. A comparison of lipase and trypsin encapsulated in mesoporous materials with varying pore sizes and pH conditions. *Colloids and Surfaces B: Biointerfaces.* 2011;**87**:464-471. DOI: 10.1016/j.colsurfb.2011.06.012
- [29] Wang C, Zhou G, Xu Y, Chen J. Porcine pancreatic lipase immobilized in amino-functionalized short rod-shaped mesoporous silica prepared using poly(ethylene glycol) and triblock copolymer as templates. *Journal of Physical Chemistry C.* 2011;**115**:22191-22199. DOI: 10.1021/jp206836v
- [30] Chen Y, Chen Q, Song L, Li HP, Hou FZ. Preparation and characterization of encapsulation of Europium complex into meso-structured silica monoliths using PEG as the template. *Microporous and Mesoporous Materials.* 2009;**122**:7-12. DOI: 10.1016/j.micromeso.2008.12.021
- [31] Cao L. Immobilised enzymes: Science or art? *Current Opinion in Chemical Biology.* 2005;**9**:217-226. DOI: 10.1016/j.cbpa.2005.02.014
- [32] Yu WH, Fang M, Tong DS, Shao P, Xu TN, Zhou CH. Immobilization of *Candida rugosa* lipase on hexagonal mesoporous silica and selective esterification in nonaqueous medium. *Biochemical Engineering Journal.* 2013;**70**:97-105. DOI: 10.1016/j.bej.2012.10.005
- [33] Tran DT, Chen CL, Chang JS. Immobilization of *Brukholderia* sp. lipase on a ferric nanocomposite for biodiesel production. *Journal of Biotechnology.* 2012;**158**:112-119. DOI: 10.1016/j.jbiotec.2012.01.018
- [34] Mendes AA, Oliveira PC, de Castro HF. Properties and biotechnological applications of porcine pancreatic lipase. *Journal of Molecular Catalysis B: Enzymatic.* 2012;**78**:119-134. DOI: 10.1016/j.molcatb.2012.03.004
- [35] Stine KJ. Enzyme immobilization on nanoporous gold: A review. *Biochemistry Insights.* 2017;**10**:1-12. DOI: 10.1177/1178626417748607
- [36] Du X, Liu X, Li Y, Wu C, Wang X, Xu P. Efficient biocatalyst by encapsulating lipase into nanoporous gold. *Nanoscale Research Letters.* 2013;**8**(1):180. DOI: 10.1186/1556-276X-8-180